# Anti-Stokes Raman conversion in silicon waveguides

**R. Claps, V. Raghunathan, D. Dimitropoulos, and B. Jalali**

*Optoelectronic Circuits and Systems Laboratory*
*University of California, Los Angeles*
*Los Angeles, CA 90095*
*jalali@ucla.edu*

*http://www.ee.ucla.edu/labs/oecs/*

**Abstract:** The first observation of parametric down-conversion in silicon is reported. Conversion from 1542.3nm to 1328.8nm is achieved using a CW pump laser at 1427 nm. The conversion occurs via Coherent Anti-Stokes Raman Scattering (CARS) in which two pump photons and one Stokes photon couple through a zone-center optical phonon to an anti-Stokes photon. The maximum measured Stokes/anti-Stokes power conversion efficiency is $1\times10^{-5}$. The value depends on the effective pump power, the Stimulated Raman Scattering (SRS) coefficient of bulk silicon, and waveguide dispersion. It is shown that the power conversion efficiency is a strong function of phase mismatch inside the waveguide.

©2003 Optical Society of America

**OCIS codes:** (230.7370) Waveguides; (250.3140) Integrated optoelectronic circuits; (250.4480) Optical amplifiers.

## References and Links

1. James B. Kuo and Shih-Chia Lin, *Low voltage SOI CMOS VLSI circuits and devices*, John Wiley and Sons, Incorporated, 2001, ISBN 047-1417777.
2. M. Cardona, G. Guntherodt, *Light Scattering in Solids II*, in *Topics in Applied Physics*, Vol. 50. Chapter 4, "Coherent and Hyper-Raman Techniques," by H. Vogt. (Springer-Verlag, Berlin, 1982). ISBN 0-387-11380-0.
3. M.C. Ho, K. Uesaka, Michel Marhic, Y. Akasaka, L.G. Kazovsky, "200-nm-Bandwidth Fiber Optical Amplifier Combining Parametric and Raman Gain," J. Lightwave Technol. **19**, 977-981 (2001).
4. M.E. Marhic, K.K.-Y. Wong, and L.G. Kazovsky, "Prospects for CW Fiber OPAs and OPOs," Proceedings CLEO (Optical Society of America, Washington, D.C., 2003) CTuA1.
5. J.K. Chee, J-M Liu, "Polarization-Dependent Parametric and Raman Processes in a Birefringent Optical Fiber," IEEE J. Quantum Electron. **26**, 541-549 (1990).
6. Y.R. Shen, N. Bloembergen, "Theory of Stimulated Brillouin and Raman Scattering," Phys. Rev. A **137**, A1787-A1805 (1964).
7. E. Golovchenko, P. V. Mamyshev, A. N. Pilipetskii, E.M. Dianov, "Mutual Influence of the Parametric Effects and Stimulated Raman Scattering in Optical Fibers," IEEE J. Quantum Electron. **26**, 1815-1820 (1990).
8. P.A. Temple, C.E. Hathaway, "Multiphonon Raman Spectrum of Silicon," Phys. Rev. A **7**, 3685-3697 (1973).
9. J.M. Ralston, R.K. Chang, "Spontaneous-Raman-scattering efficiency and stimulated scattering in silicon," Phys. Rev. B **2**, 1858-1862 (1970).
10. R. Claps, D. Dimitropoulos, Y. Han, B. Jalali, "Observation of Raman emission in silicon waveguides at 1.54 μm," Opt. Express **10**, 1305-1313 (2002). http://www.opticsexpress.org/abstract.cfm?URI=OPEX-10-22-1305
11. R. Claps, D. Dimitropoulos, V. Raghunathan, Y. Han, B. Jalali, "Observation of Stimulated Raman Scattering in Silicon Waveguides," Opt. Express **11**, 1731-1739 (2003). http://www.opticsexpress.org/abstract.cfm?URI=OPEX-11-15-1731
12. D. Dimitropoulos, B. Houshmand, R. Claps, B. Jalali, "Coupled-mode theory of the Raman effect in Silicon-On-Insulator waveguides," Optics Letters **28**(20) 1954-1956 (2003).
13. J.J. Wynne, "Optical Third-Order Mixing in GaAs, Ge, Si, and InAs," Phys. Rev. **178** 1295-1303 (1969).

#2876 - $15.00 US Received August 08, 2003; Revised October 23, 2003
(C) 2003 OSA

14. H.K. Tsang, C.S. Wong, T.K. Lang, I.E. Day, S.W. Roberts, A. Harpin, J. Drake, M. Asghari, "Optical dispersion, two-photon absorption and self-phase modulation in silicon waveguides at 1.5 μm wavelength," Appl. Phys. Lett. 3, 416-418 (2002).
15. Spectra-Physics Telecom: "Model RL5 Raman Fiber Laser Specifications".

## 1. Introduction

The study of nonlinear optical materials has been driven in recent years by the need of optically active devices that can be monolithically integrated into optoelectronic circuits. Silicon offers the capability of optoelectronic integration via Silicon-On-Insulator (SOI) technology [1]. The major limitation of silicon, in this context, has been the lack of mechanisms for light generation, amplification, and wavelength conversion. Hence, the study of optical nonlinearities in silicon waveguides is of importance to determine the feasibility of realizing SOI-based optoelectronic circuits, with both passive and active optical functionality.

Coherent Anti-Stokes Raman Scattering (CARS), Parametric Wavelength Conversion (PWC), and Optical Parametric Amplification (OPA) are well-known nonlinear optical processes [2, 3]. PWC and OPA have been extensively investigated in optical fibers in the context of broadband signal amplification, or as wavelength-conversion mechanisms [4,5]. The theory that governs these phenomena has been fully developed in the past [6]. Considering only the $\chi^{(3)}$ component of the optical interaction and assuming no pump power depletion, a detailed theory describing the interaction of Stokes and anti-Stokes waves via SRS and Four Wave Mixing (FWM) has been developed [7]. The present situation involves interaction of three fields: the pump, the Stokes, and the anti-Stokes (a-Stokes) fields, at wavelengths (frequencies) $\lambda_p(\omega_p)$, $\lambda_S(\omega_S)$, $\lambda_{aS}(\omega_{aS})$, respectively. These fields interact inside a SOI waveguide via the third-rank nonlinear tensor of silicon ($\chi^{(3)}$). In what follows, for the sake of simplicity and to accurately describe the conditions of the experiments performed, it will be assumed that the a-Stokes field, $\mathbf{E}_{aS}$, has zero value at the front facet of the waveguide. The incoming fields will be the pump, $\mathbf{E}_P$ ($TE_0$ mode), and the Stokes, $\mathbf{E}_S$ ($TM_0$ mode). In general, the $\chi^{(3)}$ tensor has two contributions. The first is the "electronic", non-resonant component, $\chi^{(3)}_{NR}$, which is nearly instantaneous in response and hence broadband, and which accounts for such effects as self-phase modulation (SPM) and FWM. The second is the Raman component, $\chi^{(3)}_R(\Omega=\omega_p-\omega_S)$ which accounts for SRS. The $\chi^{(3)}_R(\Omega)$ component has a strong spectral dependence, with a resonant peak at $\Omega=\Omega_0$, the frequency of oscillation of zone-center optical phonons in silicon. The element $\chi^{(3)}_R(\Omega)$ has therefore the spectral signature of the Raman-active phonon modes of vibration of the crystal lattice. This implies that there is a response time associated with this component, which corresponds to the phonon de-phasing lifetime. In the case of first order Raman scattering from silicon at room temperature, where only zone-center optical phonons are involved, the bandwidth is ~ 105 GHz. This corresponds to a response time of about 10 ps. In this paper we demonstrate, for the first time, Stokes to anti-Stokes wave-conversion in silicon waveguides. A detailed presentation of the experimental results will be given, plus a qualitative description of the physics involved. The wavelength-conversion phenomenon is reminiscent of coherent anti-Stokes generation (CARS) under quasi-phase-matching conditions. Wavelength conversion has important implications for optical communication, in particular for optical packet routing. In the following section, a brief theoretical review of SRS and Stokes/anti-Stokes wave coupling in silicon will be presented. The results that are relevant to the experimental conditions of the present work will be highlighted, followed by the description of the experimental work in Section 3.

#2876 - $15.00 US Received August 08, 2003; Revised October 23, 2003
(C) 2003 OSA

## 2. Background

The spontaneous and stimulated Raman scattering in bulk silicon and in the visible region of the spectrum have been studied in the past [8, 9]. Recently, our group has reported the first observation of spontaneous [10] and stimulated [11] Raman scattering in integrated silicon waveguides. In addition, we have performed a detailed coupled-mode analysis of SRS in silicon waveguides [12]. The waveguides used in our previous measurements and in the current setup were fabricated parallel to $[1\bar{1}0]$ direction on a silicon $[001]$ surface, due to the favorable cleaving property of silicon in this orientation. This geometry lends itself to a coordinate system $(x, y, z)$ rotated with respect to the crystallographic axes by 45° around the $[001]$ axis. In this system, the waveguide is oriented along the z-axis, the $TM_0$ mode is linearly polarized along the Y-axis, and the $TE_0$ mode along the X-axis. The tensorial nature and symmetry properties of $\chi^{(3)}_R(\Omega)$ in silicon are inherited from the spontaneous Raman tensor, and is carried in the three Raman tensor components, $R_i$, which in the present coordinate system are written as [12],

$$\vec{\vec{R}}_1 = \frac{1}{\sqrt{2}}\begin{pmatrix} 0 & 0 & 1 \\ 0 & 0 & 1 \\ 1 & 1 & 0 \end{pmatrix}; \quad \vec{\vec{R}}_2 = \frac{1}{\sqrt{2}}\begin{pmatrix} 0 & 0 & 1 \\ 0 & 0 & -1 \\ 1 & -1 & 0 \end{pmatrix}; \quad \vec{\vec{R}}_3 = \begin{pmatrix} 1 & 0 & 0 \\ 0 & -1 & 0 \\ 0 & 0 & 0 \end{pmatrix} \tag{1}$$

The anisotropic scattering efficiency, $S(\Omega)$, defined as the percentage of scattered radiation per unit of solid angle, per unit length, is related to the Raman tensor as follows

$$S(\Omega) = S_o(\Omega) \sum_{n=1,2,3} \left| \hat{e}_s \cdot \vec{\vec{R}}_n \cdot \hat{e}_i \right|^2 , \tag{2}$$

where $\hat{e}_i, \hat{e}_s$ are the polarizations of the incident and scattered radiation, respectively. $S_o(\Omega)$ is a constant of proportionality that contains the material parameters. The value of $S(\Omega)$ at the peak Raman shift ($\Omega$=15.6 THz) was measured to be 4.1 x $10^{-7}$ cm $^{-1}$Sr $^{-1}$ [10]. For the stimulated Raman effect in bulk material, the gain coefficient $g_s$, is obtained from the spontaneous efficiency following reference [9].

The relevant parameters for SRS and FWM in silicon can be summarized as,

$$\Omega = \omega_p - \omega_s; \quad \Omega_0 = 15.6 \text{ THz}, \tag{3.1}$$

$$\begin{aligned} g_s(\Omega_0) &= \frac{8\pi c^2 \omega_p}{\hbar \omega_s^4 n^2(\omega_s)(N+1)\Delta\omega} S(\Omega_0) \\ &= -i\,4\pi\, \chi_R^{(3)}(\Omega_0)\, \omega^2/(c^2 k) \\ &= 3.7\times 10^{-8}\ cm/W, \end{aligned} \tag{3.2}$$

$$R = 2\pi\, \chi_{NR}^{(3)}\, \omega^2/(c^2 k) = 1.7\times 10^{-9}\ cm/W. \tag{3.3}$$

Where $N$ is the Bose occupation factor (0.1 at room temperature), $n$ is the refractive index, and $\Delta\omega$ is the FWHM of the spontaneous Raman line-shape. Equation (3.2) defines the Raman susceptibility, $\chi^3_R$. In Eq. (3.3), the value of $\chi^{(3)}_{NR}$ is the $\chi_{1221}$ component of the nonlinear susceptibility tensor [13, 14]. For a waveguide along the Z-axis, the amplitude of

#2876 - $15.00 US Received August 08, 2003; Revised October 23, 2003
(C) 2003 OSA

the Y-axis component ($TM_0$ mode) of the anti-Stokes field, $E_{aS}(z)$, is related to the initial amplitude of the Y-axis component ($TM_0$ mode) of the Stokes field, $E_{So}$, by [7]

$$E_{aS}(z) = -i\, e^{i(\Delta k + RI_p)\cdot z/2} \cdot (2R + ig_s(\Omega))I_p \cdot \frac{\sinh Az}{2A} \cdot E_{So}. \tag{4}$$

Where $I_p$ is the effective pump intensity and $\Delta k$ is the phase mismatch between pump, Stokes and anti-Stokes waves, defined as,

$$\Delta k = 2k_p^{TE} - k_S^{TM} - k_{aS}^{TM} \quad . \tag{5}$$

Note that in Eq. (5), the phase difference takes into account the two different polarization modes in the waveguide ($TE_0$ and $TM_0$) and therefore, waveguide-induced birefringence will play a crucial role in the efficiency of Stokes to anti-Stokes conversion. The coefficient *A*, in Eq. (4), is given by [7]

$$A = \sqrt{(2R + ig_s(\Omega))I_p \cdot (\Delta k/2) - (\Delta k/2)^2}\,. \tag{6}$$

Note that *A* is in general a complex number. Its real part is responsible for an exponential gain in the a-Stokes wave [7]. The imaginary part of *A* results in an oscillatory behavior of the a-Stokes conversion efficiency, along the waveguide direction, z. As will be shown in Figure 1, it also manifests itself as a characteristic $\mathrm{sinc}^2$ dependence of the a-Stokes power on the phase mismatch. From Eqs. (4) and (6), two regimes can be clearly identified,

$$\begin{aligned} |\Delta k| \quad &>> \quad |4R + 2g_s(\Omega)|\, I_p, \\ |\Delta k| \quad &<< \quad |4R + 2g_s(\Omega)|\, I_p\,. \end{aligned} \tag{7}$$

The first case corresponds to an SRS dominated regime in which the large phase mismatch diminishes the FWM efficiency. In this regime, the Stokes signal is exponentially amplified with pump power and waveguides length, and the generated a-Stokes wave is negligible. The second case corresponds to a nearly phase-matched condition, in which the anti-Stokes signal is linearly amplified via the FWM effect. This process depletes the pump wave, effectively suppressing the exponential SRS gain. With the values given in Eq. (3) for the nonlinear coefficients in silicon, and assuming an effective pump power of 0.7 W inside the waveguide, the value of the threshold that defines these two regimes is

$$|4R + 2g_s(\Omega)|\, I_p \;=\; 2.1\, cm^{-1}. \tag{8}$$

Therefore, to operate the waveguide as an amplifier, the amplitude of $\Delta k$ must be larger than 2.1 $cm^{-1}$, whereas to realize efficient wavelength conversion, the phase mismatch must have much smaller amplitude than 2.1 $cm^{-1}$. Figure 1 shows the Stokes to anti-Stokes conversion efficiency vs. $\Delta k$, calculated using Eq. (4). The efficiency has a $\mathrm{sinc}^2$ dependence on $\Delta k$, for all values larger than the threshold defined in Eq. (8). At the threshold value, $\Delta k$ = 2.1 $cm^{-1}$, the conversion efficiency is approximately 0.5 %. For $|\Delta k|$ smaller than 10 $cm^{-1}$, the maximum efficiency drops by at least two orders of magnitude, compared to the phase-matched condition. From this figure, it is evident that in the SRS regime the anti-Stokes conversion efficiency is not a single-valued function of $\Delta k$. Furthermore, the lower the conversion efficiency is, the wider the range of values of $\Delta k$ that can fit it.

#2876 - $15.00 US Received August 08, 2003; Revised October 23, 2003
(C) 2003 OSA

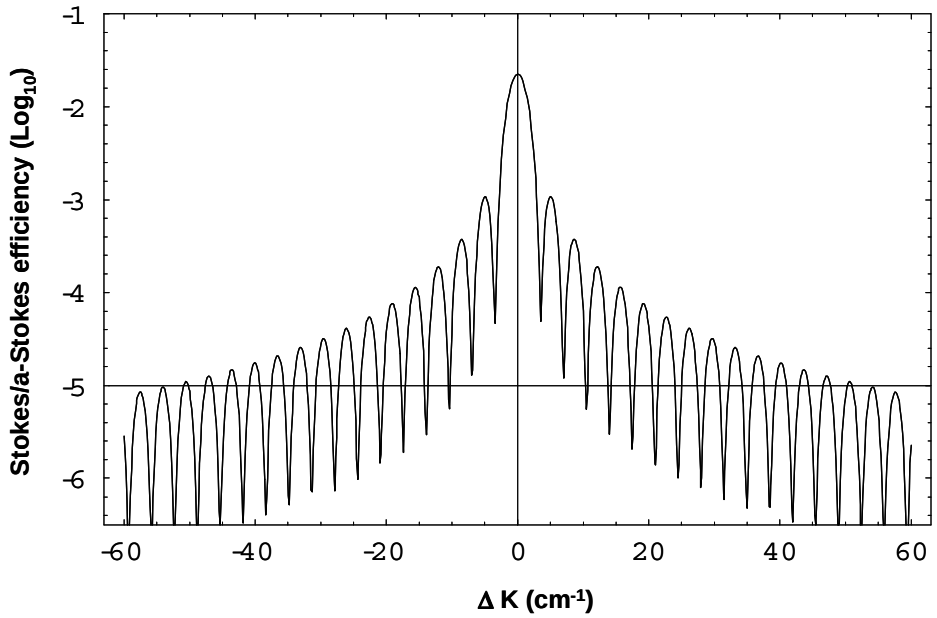


Fig. 1- Conversion efficiency, calculated from Eq. (4) using an effective pump power of 0.7 W at the input facet of the waveguide. The measured efficiency in the experiment is $1\times10^{-5}$.

Figure 2 is a plot of the real part of the coefficient *A*, relative to the value of the Raman gain, $g_s$, as a function of the phase mismatch parameter, $\Delta k$, according to Eq. (6). The plot depicts the suppression of the exponential SRS gain as the phase-matched condition ($\Delta k = 0$ $cm^{-1}$) is reached. It is also clear that the gain suppression is negligible for absolute values of the phase mismatch lower than 10 $cm^{-1}$. Also noticeable is the regime for small, positive values of $\Delta k$ (~ 1 $cm^{-1}$) in which the gain coefficient is larger than that of pure SRS. This behavior has been predicted in silica fibers and has been attributed to Modulation Instability [7].

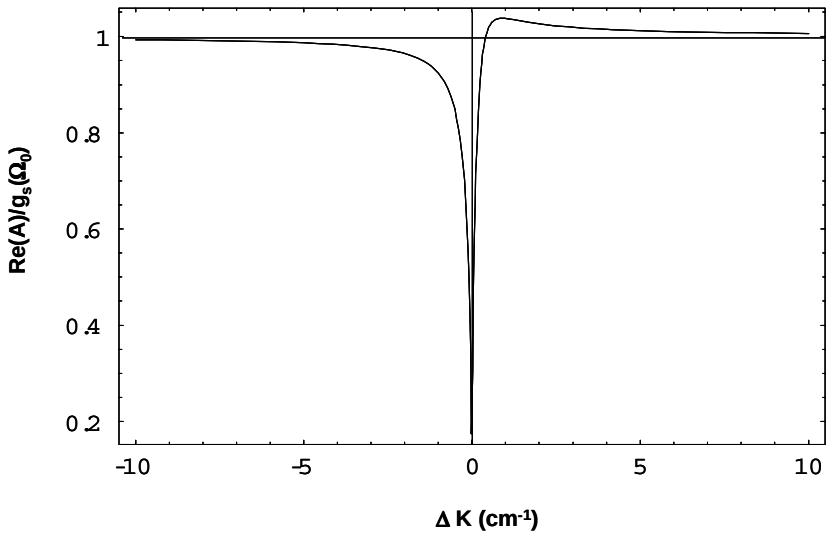


Fig. 2- Ratio of effective gain relative to SRS Raman gain, calculated from Eq. (6).

#2876 - $15.00 US Received August 08, 2003; Revised October 23, 2003
(C) 2003 OSA

## 3. Experimental setup

The experimental setup depicted in Fig. 3 is similar to the setup used to measure spontaneous Raman emission and SRS in silicon waveguides [10, 11]. The pump used is a CW, cascaded-Raman-cavity (CRC) fiber laser (Spectra Physics), operating at a wavelength of 1427 nm. The signal laser is an External-Cavity-Diode-Laser (ECDL, New Focus), tuned in the Stokes domain from 1535 nm to 1550 nm.

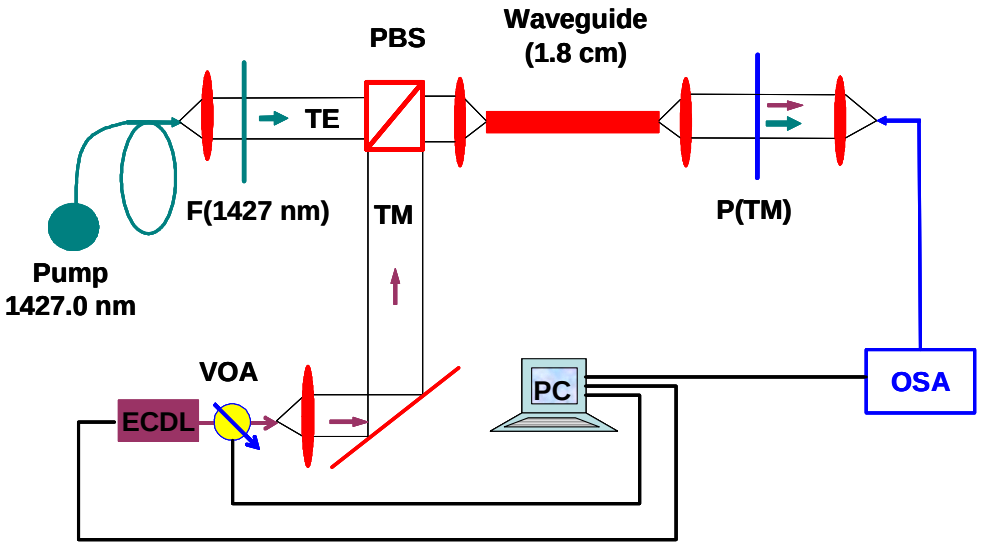


Fig. 3 Experimental setup used for observing CARS in silicon. F.- Pump laser filter. PBS.- Polarizing beam splitter. P(TM).- Polarizer to collect the $TM_0$ mode from SOI waveguide. OSA.- Optical Spectrum Analyzer. ECDL.- External Cavity Diode Laser, to use as a signal, with a scan range from 1535 to 1550 nm. VOA.- Variable Optical Attenuator.

The Polarizing-Beam-Splitter (PBS) is used to couple the pump and signal lasers into the waveguide, in a cross-polarization scheme. The pump laser is coupled into the $TE_0$ mode and the signal laser is coupled into the $TM_0$ mode. In order to measure the conversion efficiency between the Stokes and the a-Stokes signal, a Variable Optical Attenuator (VOA) is placed after the ECDL. Only the $TM_0$ mode is collected at the waveguide output. No filter for the residual pump and signal beams is necessary, since the a-Stokes signal is collected by an Optical Spectrum Analyzer (OSA). The total pump-to-waveguide coupling loss is 6.1 dB consisting of 3dB loss due to the PBS, 1dB due to the pump filter, and 2.1dB of coupling loss into the waveguide. Fabry-Perot fringes from the cavity formed between the two facets of the waveguide (which are not AR coated), are small in amplitude compared to the observed spectral signature of the CARS effect. Therefore, these fringes are irrelevant for the results presented in the following section. The waveguide had a cross section of 5.4 $\mu m^2$ and was fabricated along the $[1\,\bar{1}\,0]$ direction of silicon [11].

## 4. Results

Figure 4 shows the anti-Stokes spectra measured as a function of the Stokes laser wavelength. There is a clear peak at 1328.8nm of anti-Stokes emission when the Stokes laser is tuned to 1542.3nm. The latter corresponds to the peak of the spontaneous Raman emission in silicon. The nature of the weaker features in Fig. 4 most likely corresponds to the wavelength-dependent character of the phase-matching parameter, $\Delta k$, in the SOI waveguide. Further analysis will be carried out in the future, considering other polarization configurations of the experiment, to determine the symmetry properties of these resonances.

#2876 - $15.00 US
Received August 08, 2003; Revised October 23, 2003
(C) 2003 OSA

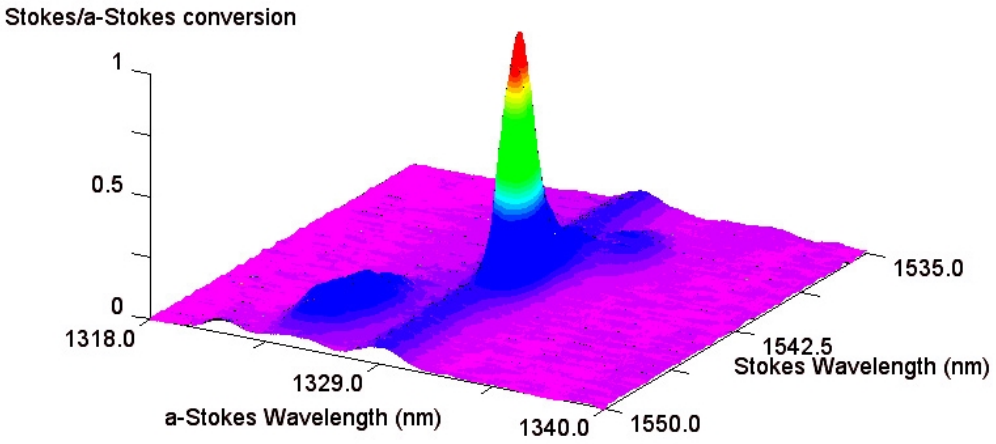


Fig. 4 Plot of the a-Stokes spectra collected for a given value of the signal (Stokes wavelength). The z-axis represents the Stokes/a-Stokes conversion efficiency, normalized to unity. Note the clear appearance of two "satellite" resonances, as mentioned in the text.

Figure 5 shows the a-Stokes power, integrated across the anti-Stokes spectrum (1323-1333 nm), as a function of the pump power effectively coupled into the waveguide (red triangles). The blue diamonds correspond to counter-propagating pump and Stokes signal in the waveguide. The relative lack of a-Stokes emission in the counter propagating condition underscores the importance of phase matching. In this case ($\Delta k=2.8\times10^4$ $cm^{-1}$), any a-Stokes signal would be due to down-converted spontaneous Stokes emission. Also shown in the figure is the measured power when the Stokes laser is off (crosses). The relative absence of power in this case is an unambiguous indication that the measured a-Stokes signal is that of down-converted Stokes signal. The figure also shows the result for the a-Stokes power obtained from Eq. (4) (solid line) using $\Delta k \sim -27$ $cm^{-1}$. The fact that the theoretical fit spans several values of a-Stokes power reduces the range of $\Delta k$ values that match the measured data. Nonetheless, it should be stressed that the above procedure will not be construed as an accurate measurement of $\Delta k$. The latter can be achieved using procedures similar to those outlined in reference [14].

#2876 - $15.00 US Received August 08, 2003; Revised October 23, 2003
(C) 2003 OSA

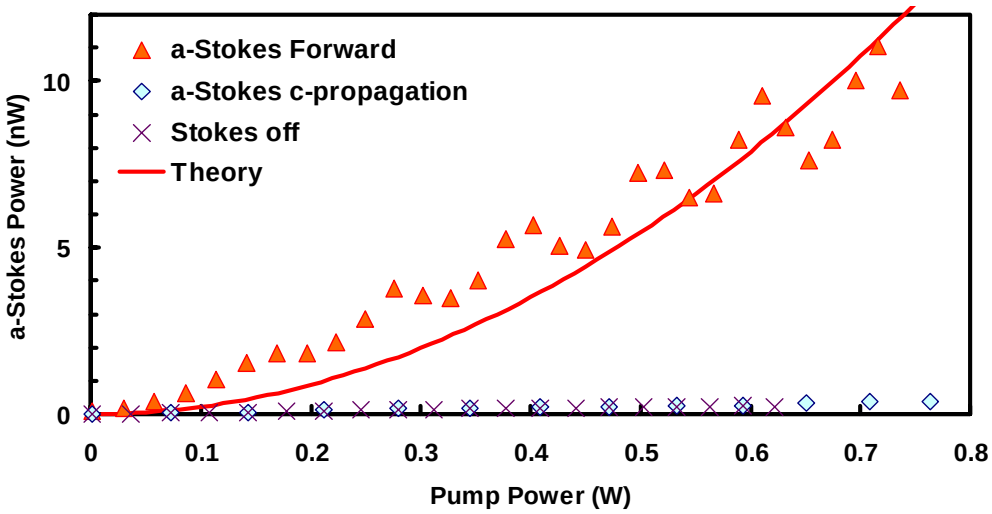


Fig. 5.- Integrated a-Stokes power signal vs. pump power, with the Stokes signal power fixed. The integration is carried out from 1323 to 1333 nm in the a-Stokes spectra (Fig. 4). The red triangles show clearly the a-Stokes amplification due to Stokes parametric down-conversion. The blue diamonds correspond to counter-propagating pump and Stokes signal in the waveguide. The crosses are the down-converted, spontaneous a-Stokes signal. The Stokes signal was set at 1542.3 nm and 300 μW of input power. The fit with Eq. (4) was performed using A = $\sqrt{-179-2.3i}$ . This corresponds to $\Delta k \sim -27\ cm^{-1}$.

Figure 6 shows the integrated power in the a-Stokes domain as a function of the Stokes wavelength, $\lambda_s$. The peak shown at the center of the Raman frequency shift (1542.3 nm) indicates that the observed parametric down conversion has the spectral characteristic of Stimulated Raman emission in silicon, as expected from Eq. (4). Note that at high pump powers, the data appears to show a double-peak spectrum. The reason for this is that at high powers, the pump laser exhibits a double-peak spectral line-shape. This is a well known artifact of CRC fiber lasers, and is well documented by the manufacturer [15]. To obtain the down-conversion efficiency, the a-Stokes integrated power was measured as a function of the Stokes signal power, for different values of pump power. The result is shown in Fig. 7.

#2876 - $15.00 US
Received August 08, 2003; Revised October 23, 2003
(C) 2003 OSA

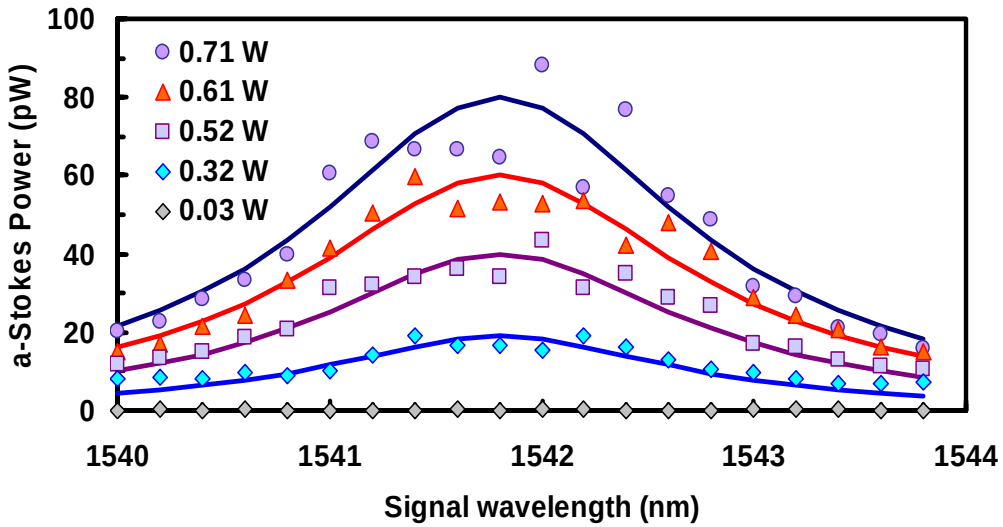


Fig. 6.- Spectral dependence of the a-Stokes integrated power (as in Fig. 4), against Stokes wavelength, for different values of pump power. The solid lines are lorentzian fits to the data. Data fluctuation at high pump power in the region close to the Raman resonance (1542.3 nm) is most likely due to Fabry-Perot effects from the waveguide facets [11].

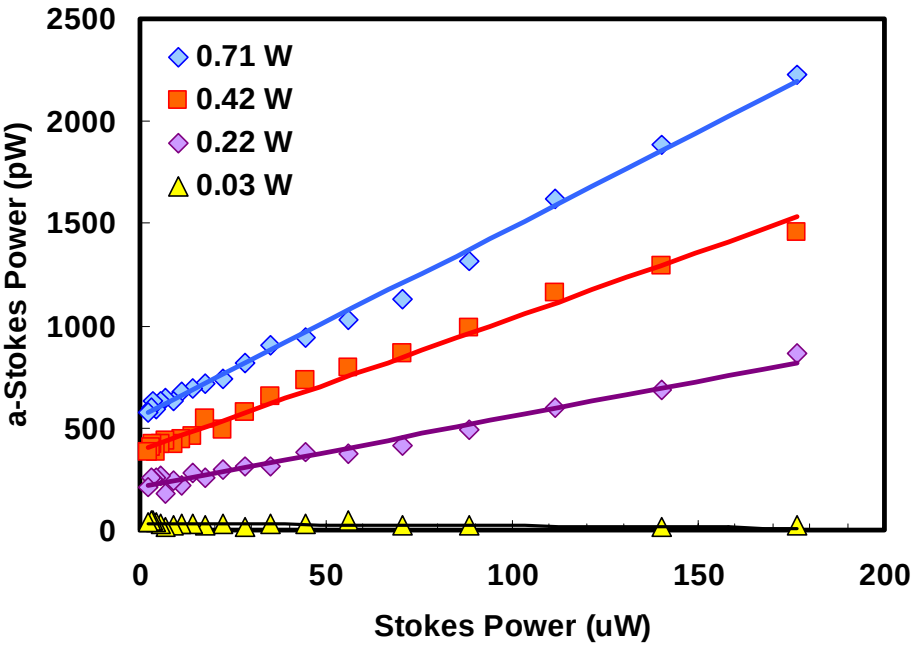


Fig. 7. Stokes to a-Stokes conversion efficiency. The Stokes power was varied using the VOA shown in Fig. 3. The efficiency, defined as the slope of the plots shown, increases with pump power, as expected from Eq. (4).

#2876 - $15.00 US
Received August 08, 2003; Revised October 23, 2003
(C) 2003 OSA

From the slopes in Fig. 7, the maximum Stokes/anti-Stokes power conversion efficiency measured for this particular waveguide is found to be $1\times10^{-5}$, for an effective pump power of 0.7 W. Referring to Fig. 1, the horizontal line shows the measured conversion efficiency relative to the phase mismatch parameter. Because of the oscillatory nature of the curve, an accurate estimation of the phase-mismatch, based on the measured CARS efficiency, is not possible when the efficiency is low. Specifically, the values of $\Delta k$ that match the measured conversion efficiency are in the range -55 to -10 $cm^{-1}$.

Next, an Erbium-Doped-Fiber-Amplifier was introduced in the setup, to amplify the Stokes signal up to 20 mW. The result is an effective signal power of about 5 mW inside the waveguide, leading to a maximum a-Stokes signal observed of 55 nW, as shown in Fig. 8.

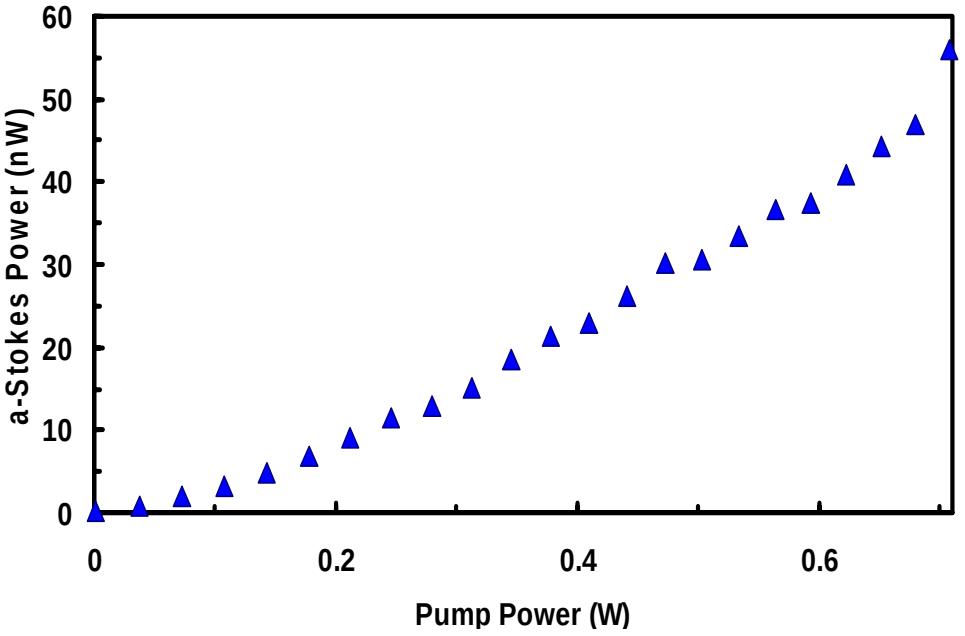


Fig. 8. Maximum amount of a-Stokes signal obtained, at 1328.8 nm. It was obtained by increasing the Stokes signal power up to ~ 5 mW effectively coupled into the waveguide.

## 4. Conclusions

This paper has reported the first observation of coherent anti-Stokes Raman scattering in silicon. Specifically, we have demonstrated coherent parametric wavelength conversion from 1543.3nm to 1328.8 nm. This was achieved using a 1427nm CW pump with ~2nm linewidth. The bandwidth over which the conversion occurs corresponds to that of the Raman process. Including the pump broadening effect, this bandwidth is 350GHz in the present experiment. The bandwidth may be increased using multiple pumps, suitably spaced in wavelengths. The measured Stokes / anti-Stokes power conversion efficiency is $1\times10^{-5}$. The relatively low conversion efficiency can be attributed to the non-phase-matched condition in the present waveguide. With proper design of waveguide dispersion, conversion efficiency can be drastically increased, leading to silicon based, all-optical wavelength converters, suitable for optical packet switched networks.

#2876 - $15.00 US Received August 08, 2003; Revised October 23, 2003
(C) 2003 OSA

**Acknowledgments**

This work was supported by the MTO office of the Defense Advance Research Project Agency (DARPA). The authors would like to thank Dr. Jag Shah for his support.

#2876 - $15.00 US Received August 08, 2003; Revised October 23, 2003
(C) 2003 OSA